AIAA JOURNAL
Vol. 47, No. 10, October 2009

Modeling and Analysis of Semi-Active Dampers in Periodic Working Environments

Branislav Titurus* and Nick Lieven†
University of Bristol, Bristol, England BS8 1TR, United Kingdom

DOI: 10.2514/1.41774

This paper develops the concept of the semi-active hydraulic damper representing the control component assumed to be located in the periodic working environment. The assumption of the periodic working environment is applicable for a wide range of vibration-related applications. Within a specified framework, a reduced-order physically based mathematical model of the damper is established using realistic assumptions and concepts from the hydraulic system theory. A general need for damper activity parameterization is considered, retaining the periodic nature of the application, and the two specific parameterization instances are considered: a local piecewise polynomial and a global multiharmonic activity parameterization. This device is further demonstrated in simulated case studies based on realistic values of physical devices. The activity of the damper is assumed to be based on the periodic modulation of the size of the flow restrictor located between two working chambers of the damper. The general physical effects associated with the damper operation in this working mode are investigated and explained for both types of damper activity parameterizations.

Nomenclature

A_P	=	cross-sectional area of the symmetric piston
A_{PV}	=	pseudosection function
A_V	=	cross-sectional area of the valve opening
B_0	=	constant bulk modulus of a hydraulic fluid
C_D	=	discharge coefficient
c_D	=	coefficient of a general algebraic model of the damping force
D_1, D_2	=	linear and quadratic flow-pressure coefficients
$\mathcal{D}_\psi$	=	azimuth angle domain, $[0,\ 2\pi]$
d_O	=	diameter of the circular orifice
$d(\circ)/dt$	=	time derivative, $(\dot{\circ})$
$d(\circ)/d\psi$	=	spatial or azimuth derivative, $(\circ)'$
F_D	=	damper force
$\mathbf{f}(\circ)$	=	damper state-space model
$g(\circ)$	=	nonlinear response generator function
$\mathcal{I}$	=	set of damper inputs
K	=	composite discharge constant
$\dot{m}$	=	mass flow rate
N_D	=	number of the damper model states
N_P	=	number of the parameters used in the activity parameterization
N_V	=	total number of valve physical parameters
$\mathcal{P}$	=	activity parameterization family
p	=	absolute and homogeneous pressure in the fluid container
$\mathbf{p}$	=	vector of the parameters used in the activity parameterization
$\mathbf{p}_V$	=	vector of the valve parameters
$p_{V,A,i}$	=	value of the ith active valve parameter
Q	=	volumetric flow rate
q^{-1}	=	inverse of the function q
$q(\circ)$	=	flow pressure static characteristics
$\mathcal{R}$	=	set of observed damper outputs
Re	=	Reynolds number
r	=	generic output response quantity
$\text{sign}(\circ)$	=	signum function
$\mathcal{U}$	=	set of discharge coefficient factors of the controllable flow-restricting element
$\bigcup[\circ]$	=	union of the intervals
u	=	absolute value of the (control) variable of the controllable flow-restricting element
V	=	volume of the fluid chamber
W_{PC}	=	work done per one cycle of the damper operation
χ_j	=	local polynomial of the activity parameterization family $\mathcal{P}_\chi$
$\mathbf{x}$	=	state vector
xR	=	number of cycles per one revolution
x_V	=	valve spool displacement
$x\Omega$	=	angular frequency represented as an integer multiple of the rotating frequency
y_P	=	piston displacement
α	=	exponent of the polynomial representation of the inverse flow-pressure characteristics
β	=	isothermal tangent compressibility of the hydraulic fluid
Δp	=	pressure difference due to pressure losses
η	=	fluid dynamic viscosity
λ	=	ratio of the initial volumes of the damper working chambers
$\bar{\pi}$	=	scaled quantity π
ρ	=	density of hydraulic fluid
ψ	=	azimuth angle
Ω	=	fundamental angular frequency
$\lvert\circ\rvert$	=	absolute value

Received 23 October 2008; revision received 28 May 2009; accepted for publication 14 June 2009.

*Research Associate, Department of Aerospace Engineering, Queens Building, University Walk.

†Professor, Department of Aerospace Engineering, Queens Building, University Walk.

I. Introduction

THIS paper provides an introductory study of the use of a hydraulic semi-active damper used for vibration suppression. This component is assumed to be placed in the periodic working environment. A specified regime can (in general) represent steady operating conditions of structures with rotating components (such as turbines), steady flight regimes of the rotary wing aircraft, and structures with propellers and rotating blades (such as ships and wind turbines), and many others. The hydraulic damper is therefore considered as a candidate solution for adaptive vibration suppression via its integration with an active component, resulting in a semi-active device. Despite this modification, the damper retains its basic

physical mechanism of operation; therefore, the term semi-active damper will be used throughout this paper.

Early references and research in the field of semi-active technologies can be traced to the late 1970s and early 1980s, with applications in the car industry. The summary of the investigation of semi-active concepts was given by Karnopp [1]. In his work, he also proposed and investigated multiple designs of semi-active damping components (as well as their limitations) used to control vibrations transmitted due to road unevenness through the car suspension system into the car chassis. A more recent study of this approach, with a focus on the modeling issues, is presented by Heo et al. in [2]. In their work, an extensive study of a continuously variable damper model based on a detailed hydromechanic modeling approach is presented. An alternative approach, based on the notch frequency localized to reduce vibration transmissivity and used for the fluid engine mount design, was presented in [3]. The research presented by Patten et al. in [4,5] traces its origins to semi-active car suspension research with later transfer of the design concepts to civil engineering applications. The use of semi-active dampers is considered in this work to increase the useful life of bridges. The application of semi-active damping technology in seismic protection is reported by Symans and Constantinou in [6].

Applications often lead to systems of the time-periodic nature, with their models represented in nonlinear, linear, or linearized time-periodic format [7,8]. This problem domain is well represented by the applications within the rotary aircraft sector, with significant effort to control or minimize vibration levels in usually extreme vibratory environments. These efforts have resulted in the design of fully active control schemes based on the principles of the higher harmonic control (HHC) theory. Within this methodology, single or multiharmonic inputs are provided to these systems such that their application modifies the original vibration patterns with an overall effort dedicated to their minimization. An early account of this approach is provided by Johnson [9], and recent theoretical analysis of HHC is provided by Patt et al. [10]. The harmonic or general periodic inputs assumed in general theoretical concept of HHC were practically proposed to be applied via an active swash plate, an active pitch link, actively controlled flaps, and active control of the structural responses [11–14]. Among these concepts, the methods based on actively controlled flaps indicate very good performance gains, as shown in [13,14]. An extensive experimental study of the combination of swash plate and active wing-flap-based vibration control systems applied to a one-fifth-scale semispan aeroelastic model of the tiltrotor V–22 was presented by Nixon et al. in [15]. In a different context, Knospe et al. [16] implemented and analyzed the use of magnetic bearings as magnetic actuators in the suppression of synchronous responses caused by rotor imbalance. Pairs of input harmonic control currents and output vibration harmonics were used in the open-loop adaptive vibration control schemes. Mettin and Kurz [17] presented an analytical study of a chaotic system with periodic control. The goal within this methodology was the use of the Fourier basis, represented by its coefficients to establish optimal periodic control parameter modulation, such that selected performance characteristics were minimized.

An alternative to HHC implementations based on fully active control concepts is a HHC methodology using semi-active control principles. Despite potentially smaller performance gains, this approach can provide an alternative to fully active or traditional passive approaches. One investigation based on this principle is the work of Anusonti-Inthra et al. [18]. In their paper, they report on a configuration with a semi-active lag and assumed flap dampers for vibration suppression. The effectiveness of the damper is suggested to be significantly influenced by the variation of the orifice size located between the two working chambers of the damper. Their study is demonstrated on the light BO–105-type helicopter during high-speed steady flight. The damper modeling and a model reduction process were motivated by the approach presented in [6]. The model of the damper used in [18] within the framework of the rotor aeroelastic code was a reduced-order model of the damper, representing an equivalent viscous damper model with a variable damping coefficient. The current paper and the research presented here is inspired by this work. Alternative considerations related to semi-active lag dampers are presented in [19,20]. Kamath et al. [19] presented a comparative study of magnetorheological and fluid-elastomeric lag dampers with a focus on modeling, identification, and component-level performance issues. Zhao et al. [20] studied helicopter ground resonance issues for the cases with controllable magnetorheological lag dampers.

While presenting the damper based on identical concept to the one presented in [18], the current contribution attempts to address the given problem and reduce the computational and modeling abstractions to a minimum. The hydraulic damper with an active orifice or other flow-controlling component is assumed and modeled on the basis of hydraulic system theory. This approach is used for analysis and demonstrated via analytical case studies. The objective of the paper therefore is to present initial reasoning, mathematical modeling, and introductory analysis assuming a damper's periodic modulation or control and its operation in periodic working environment with the same fundamental frequency. The vibration suppression application itself is not included here as the current paper serves to provide treatment of underlying concepts that can be used later in a wider and application-specific context.

An introduction to the subject and references providing an overview of the broader context of damper modeling and HHC-based applications are provided in Sec. I. Section II introduces the theoretical and modeling framework employed in the case studies. The semi-active mode of the damper's operation is described in Sec. III, and the two control signal parameterizations are presented in Sec. IV. Section V presents case studies demonstrating the effect of the active component on the overall damper performance and the frequency response content.

II. General Modeling Arguments

In this section, a concept of the lag damper is briefly used to introduce general modeling observations and arguments associated with hydraulic dampers. This component can be assumed as a suitable representative of the damping devices working in a previously specified periodic working environment. The general modeling issues associated with this production component were part of investigations presented in works [21,22]. Novel types of lag dampers are magnetorheological fluid-elastomeric dampers [23] and magnetorheological dampers [24].

The primary role of the lag damper is stabilization of blade movement in its lead-lag plane. The need to employ separate, traditionally discrete devices is primarily relevant in the transient flight regimes (such as helicopter takeoff and landing with the well-known problem of ground resonance). Thus, the lag damper provides an additional mechanism of the energy dissipation during these scenarios. General expectation in this case is that the damper will produce high motion resisting forces, even for relatively small blade lag velocities, to ensure stability requirements. To avoid excessive load transfer into the blades and the rotor hub, the damper forces have to be restricted to structurally acceptable limits via secondary bypass flowpaths in the damper with the relief valves set up to activate when the limit forces are reached. This effect is demonstrated in Fig. 1 for

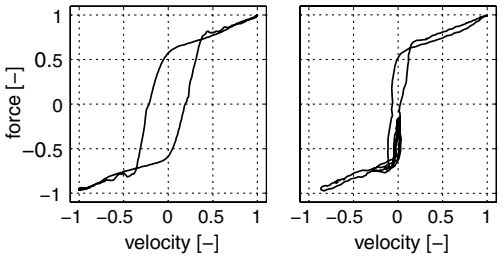

Fig. 1 One cycle of experimental records of lag damper in action from: a) a test rig with harmonic displacement excitation and b) flight tests (both data sets scaled).

one cycle of a damper's operation. The damper force is shown in the velocity-force domain for the flight-test and the laboratory-test conditions. As is shown in this figure, a steep rise in the damper force caused by a single small orifice is followed by significantly reduced force increase induced by the activation of the secondary flowpaths.

Figure 1 demonstrates the presence of considerable hysteresis effects in the velocity-force domain represented by the nonzero area determined by the line corresponding to a single cycle during steady damper operation. Figure 1a shows one velocity-force cycle acquired during laboratory tests with the prescribed harmonic excitation of the damper piston, and Fig. 1b presents the characteristics in the same domain acquired during the flight tests. In both subplots, the vertical and horizontal coordinates are scaled with respect to the maximum values of the corresponding signals. The hysteretic behavior of the damper force can be related to the compressibility effects of real hydraulic fluids containing a finite amount of air as well as finite stiffness within the damper's structural components (such as the cylinder walls and the elastic bearings) [22].

Consequently, the damper may show considerable velocity-force hysteresis that is demonstrated by 1) partial springlike energy storage and time-localized instantaneous positive power flow to the system; 2) smaller and smoothed-force peaks as responses to the extreme velocities; and 3) lagging or delayed force response. Modeling approaches exist that can generate physically based parametric models of these devices while reflecting on these observations that use standard hydraulic system theory assumptions (e.g., [25]).

III. Baseline Semi-Active Damper Model

A fixed or variable fluid volume with a number of inflow and outflow fluid paths is assumed to be filled with a compressible fluid. This approach can take into account the effect of compressibility and is traditionally used in hydraulic actuator modeling. An early reference applying these principles to linear hydraulic actuator modeling is described by Mitchell and Johnson [26]. A more recent study of the use of this modeling approach in the hydraulic actuator control context is presented by Yao et al. [27]. An application of this methodology to a model motorcycle damper was given in [28]. A detailed modeling study and experimental validation of the hydraulic model of a vehicle shock absorber is presented in [29]. Contiguous to these references, a passive lag damper with relief valves was originally modeled using this methodology by Eyres in [21]. A simple model of the damper considered in our studies is shown in Fig. 2.

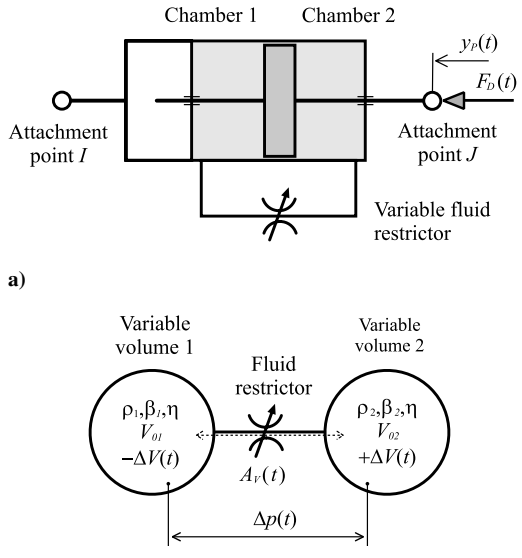

Fig. 2 Semi-active damper with through rod and variable fluid restrictor.

The damper depicted in Fig. 2 consists of four main functional parts: two chambers created by division of the cylinder by the piston head, a moving symmetric piston, and a flowpath connecting the two chambers with a variable opening representing the active fluid restrictor. The general operating principle of the damper is based on the occurrence of the pressure differential between the two chambers due to energy conversion when piston-induced fluid flow has to overcome local flowpath obstacles represented by designed and/or controlled fluid restrictors such as the orifice. The force induced by the damper is then approximately proportional to this pressure differential.

Figure 2b shows hydraulic components and the quantities of the model of the damper in which $\Delta p(t)$ is the pressure differential and the parameters ρ, β, and η denote the fluid density, the effective compressibility, and the dynamic viscosity, respectively. The damper is assumed to be filled with standard hydraulic fluid (i.e., $\beta \neq 0$). V_0 and $\pm\Delta V(t)$ denote the initial volume and the volumetric changes, respectively. The indices 1 and 2 are used to distinguish the two chambers. The variable fluid restrictor is assumed to represent the active element of the damper with a controllable orifice area A_V.

A. Hydraulic Modeling of the Damper with Compressible Fluid

The movement of the piston forces fluid flow between the two chambers such that the resulting volumetric changes have to be accommodated by the available flowpaths. These paths include flow-restricting features allowing only limited fluid transfer that can be characterized by the functional relationship $Q = q(\Delta p)$ [25], in which Q is the volumetric flow rate through the flow-restricting element and Δp is the pressure difference across the element. When the compressibility effects within the flow-restricting element are considered, more complicated mass flow characteristics should be applied [5]. The relationship $Q = q(\Delta p)$ represents the static characteristic of the flow-restricting element. A combination of the physical mechanisms can be attributed to a single physical realization of the flow restrictor (e.g., orifice) in which these can be arranged in a series such that

$$\Delta p = \sum_{(\pi)} \Delta p_\pi$$

or in parallel such that

$$Q(\Delta p) = \sum_{(\pi)} Q_\pi(\Delta p)$$

or in their combination, in which the index/label π covers all specific loss mechanisms for the given element. An example is the approach in the long orifice in which the pressure differential across the orifice corresponds to the pressure losses due to the fluid flow through this orifice. Thus, pressure differential can be assumed in the form

$$\Delta p = \Delta p_{\text{lam}} + \Delta p_{\text{turb}} = q_{\text{lam}}^{-1}(Q_O) + q_{\text{turb}}^{-1}(Q_O)$$

in which the laminar and the turbulent pressure-loss mechanisms are assumed to be arranged in a series, q_π^{-1} is the inverse static characteristic, Δp_{lam} represents the pressure loss due to laminar flow, Δp_{turb} is the pressure loss due to turbulent flow, and Q_O is the volumetric flow rate through the orifice. This model represents a considerable abstraction of real situation and possible pressure-loss scenarios across the range of the flow conditions.

Generally in dampers, due to their high-pressure nature, the compressibility of the fluid β is an important parameter. It represents the volumetric changes of the fluid under the influence of the pressure. It is also generally pressure and temperature sensitive. In this paper, an isothermal tangent fluid compressibility will be considered, and it is defined as $\beta(p)V = -dV/dp$, where V is the fluid volume and p is the homogeneous pressure of the fluid within given volume. The statement of mass conservation within single variable volume $V_i(t)$ can be expressed as $\dot{m} = \dot{m}_{\text{in}} - \dot{m}_{\text{out}}$, and this relationship can be further developed for generalized ith variable

fluid volume with multiple inflows $\dot{m}_{\text{in},j}$ and outflows $\dot{m}_{\text{out},k}$ as follows:

$$\frac{\mathrm{d}m}{\mathrm{d}t} = \frac{\mathrm{d}}{\mathrm{d}t}(\rho_i V_i) = \rho_i \frac{\mathrm{d}V_i}{\mathrm{d}t} + V_i \frac{\mathrm{d}\rho_i}{\mathrm{d}t} = \sum_{(j)} \dot{m}_{\text{in},j} - \sum_{(k)} \dot{m}_{\text{out},k}$$
$$= \sum_{(j)} \rho_j Q_{\text{in},j} - \sum_{(k)} \rho_k Q_{\text{out},k} \tag{1}$$

where ρ_i, ρ_j, and ρ_k are the densities in the ith volume, jth inflow, and kth outflow path, respectively; $\dot{m}_{\text{in},j}$ and $\dot{m}_{\text{out},k}$ are the jth inflow and kth outflow mass flow rates, respectively; and $Q_{\text{in},j}$ and $Q_{\text{out},k}$ are jth inflow and kth outflow volumetric flow rates, respectively. An assumption of homogeneous fluid density within the system $\rho_i = \rho_j = \rho_k = \rho$ leads to the generic differential equation expressing the pressure evolution within the chamber under the influence of the previously mentioned factors [6,25]:

$$\frac{\mathrm{d}V_i}{\mathrm{d}t} + \beta_i(p_i) V_i(t) \frac{\mathrm{d}p_i}{\mathrm{d}t} = \sum_{(j)} Q_{\text{in},j}(\Delta p_{ij}) - \sum_{(k)} Q_{\text{out},k}(\Delta p_{ik}) \tag{2}$$

where $\beta_i(p_i)$ is the pressure-sensitive compressibility of the hydraulic oil, p_i is the absolute pressure, Δp_{ij} and Δp_{ik} are the pressure differentials between the reference ith fluid volume and jth inflow and kth outflow-related pressure sources/ports, respectively. The flow rates Q_j and Q_k are dependent on the relative pressure differentials Δp_{ij} and Δp_{ik}, respectively, where $\Delta p_{ij} = p_i - p_j$ and $\Delta p_{ik} = p_i - p_k$.

With reference to Eq. (2) and Fig. 2, equations for separate damper chambers are

$$\dot{V}_1 + \beta_1 V_1 \dot{p}_1 = -Q_{\text{out},1}, \qquad \dot{V}_2 + \beta_2 V_2 \dot{p}_2 = +Q_{\text{in},2} \tag{3}$$

Furthermore, an initial or reference piston-cylinder configuration is assumed:

$$V_1 = V_{01} - A_P y_P, \qquad \dot{V}_1 = -A_P \dot{y}_P$$
$$V_2 = V_{02} + A_P y_P, \qquad \dot{V}_2 = +A_P \dot{y}_P \tag{4}$$

where V_{01} and V_{02} are the initial or reference fluid volumes of respective damper chambers, A_P is the pressure visible piston cross-sectional area, and y_P and $\dot{y}_P$ are the time-dependent piston displacement and velocity.

This provides the initial set of two differential equations:

$$\frac{\mathrm{d}p_1}{\mathrm{d}t} = \frac{1}{\beta_1 V_1}(-\dot{V}_1 - Q_{\text{out},1}) = \frac{1}{\beta_1 V_1}\left(+A_P \frac{\mathrm{d}y_P}{\mathrm{d}t} - Q_{\text{out},1}\right)$$
$$\frac{\mathrm{d}p_2}{\mathrm{d}t} = \frac{1}{\beta_2 V_2}(-\dot{V}_2 + Q_{\text{in},2}) = \frac{1}{\beta_2 V_2}\left(-A_P \frac{\mathrm{d}y_P}{\mathrm{d}t} + Q_{\text{in},2}\right) \tag{5}$$

As only a single path for the fluid flow between the two chambers is considered, the assumption of incompressible flow leads to the relationship $Q_{\text{out},1} = Q_{\text{in},2} = Q_V$, where Q_V is the volumetric flow rate through A_V, as shown in Fig. 2.

A single-state model of the damper can be produced for the pressure differential $\Delta p = p_1 - p_2$, and its time derivative is $\Delta \dot{p} = \dot{p}_1 - \dot{p}_2$. The use of $\Delta \dot{p}$ with Eq. (5) along with the assumption of a single flow rate Q_V results in a new single-state model of the damper:

$$\frac{\mathrm{d}(\Delta p)}{\mathrm{d}t} = \left(\frac{1}{\beta(p_1) V_1(y_P)} + \frac{1}{\beta(p_2) V_2(y_P)}\right)\left[A_P \frac{\mathrm{d}y_P}{\mathrm{d}t} - Q_V(\Delta p)\right] \tag{6}$$

The loss of information about the evolution of the absolute pressures p_i necessitates the use of the pressure-insensitive compressibility factors $\beta_1 = \beta_2 = \beta_0$ or the fluid bulk modulus $B_0 = 1/\beta_0$ corresponding to the reference pressure state with $p_i = p_0$. The state model of the damper has the form

$$\frac{\mathrm{d}(\Delta p)}{\mathrm{d}t} = B_0\left(\frac{1}{V_1(y_P)} + \frac{1}{V_2(y_P)}\right)\left[A_P \frac{\mathrm{d}y_P}{\mathrm{d}t} - Q_V(\Delta p)\right] \tag{7}$$

Equation (7) represents a nonlinear nonautonomous dynamic system with a single state Δp. This state is essential for computation of the damper force approximation $F_D \approx A_P \Delta p$ while neglecting other often minor influences such as the friction and inertial forces within the damper. An alternative solution approach to a similar problem is presented in [30] for the case of a liquid spring shock absorber.

B. Assumed Model of Fluid Flow Pressure Losses

Reference model (7) requires specification of the piston motion $y_P(t)$ representing external time-dependent input to the system as well as the static characteristics $Q_V = q(\Delta p)$. The piston motion is specified explicitly as the function $y_P = f(t)$ when evaluating damper in isolation, for instance, for model validation and refinement purposes [22]. The relationship $Q_V = q(\Delta p)$ crucially influences the overall behavior of the hydraulic network, as shown in Fig. 2b. If an incompressible hydraulic medium is assumed $\beta_0 = 0$, an inverse form of this characteristic $\Delta p = q^{-1}(Q_V)$ can be directly used to formulate the force generated by the damper based on the approximation $F_D = A_P \Delta p = A_P q^{-1}(Q_V)$. The relationships for q^{-1} can be assumed in the polynomial form $q^{-1} = \text{sign}(Q_V) q_E |Q_V|^\alpha$, where sign$(\circ)$ introduces directional dependency into the characteristics. This formulation employs the assumption of a volumetric variation for incompressible fluid $Q_V = A_P \dot{y}_P$, and it leads to the statement for the damper force $F_D = A_P q^{-1}(A_P \dot{y}_P)$ or specifically, in the case of polynomial relationships,

$$F_{D,\alpha} = -\text{sign}(\dot{y}_P) c_D |\dot{y}_P|^\alpha \tag{8}$$

The damping coefficient for this polynomial model is $c_D = q_E A_P^{\alpha+1}$, and the cases of friction, linear viscous, and quadratic dampers are represented by the exponents $\alpha \in \{0, 1, 2\}$. Where $\alpha = 0$ leads to the basic model of the friction damper $F_{D,0} = -\text{sign}(\dot{y}_P) c_{D,0}$, $\alpha = 1$ results into the standard linear viscous damper $F_{D,1} = -c_{D,1} \dot{y}_P$, and the use of $\alpha = 2$ forms the quadratic damper model $F_{D,2} = -c_{D,2} \dot{y}_P |\dot{y}_P|$.

The previous approach can be extended to mixed flow models by the use of the rational polynomial formulation [31]:

$$\Delta p = \sum_{j=1}^{N_F} d_j Q_V^{k_j}$$

where N_F is the number of polynomial terms, the exponent $k_j \in \mathbb{R}$ is mostly specified between 0 and 2, and d_j depends on the flow characteristics. This general nonlinear form must be solved for Q_V, for a given Δp, such that this Q_V can be used with model (7). A directly solvable alternative can be produced for $N_F = 2$, $k_1 = 1$, and $k_2 = 2$, resulting in a quadratic relationship with an explicit form of $Q_V = q(\Delta p)$ as required by Eq. (7). The directional form of Q_V can then be written as follows [21,32]:

$$\Delta p = D_1 Q_V + D_2 Q_V |Q_V|$$
$$Q_V = \text{sign}(\Delta p)\left(-D_1 + \sqrt{D_1^2 + 4D_2 |\Delta p|}\right)/2D_2 \tag{9}$$

where D_1 corresponds to the linear loss model predominant during small flow velocities and D_2 is related to the turbulent losses dominating during high flow velocities. If $D_1 = 0$, then

$$Q_V \equiv Q_{V,q} = \text{sign}(\Delta p)\sqrt{|\Delta p|/D_2}$$

and alternatively, based on the Taylor series expansion for $\Delta p \to 0$, the flow rate is

$$Q_V(|\Delta p| \to 0) \to Q_{V,l} = \Delta p / D_1$$

The quadratic part of Eq. (9) $\Delta p_2 \equiv \Delta p_q = D_2 Q_V |Q_V|$ corresponds to the turbulent pressure losses (e.g., [25]), and D_2 in

this case could assume the form $D_2 = \rho/[2(C_D A_V)^2]$ [21,25,31], where ρ is the fluid density, A_V is the total area of the opening, and C_D is the flow discharge coefficient [25]. In general, the parameter C_D depends on the number of flow characteristics such as the Reynolds number Re, the opening/orifice topology, dimensional configuration, etc. [31].

Whereas the previous model of the damper force $F_{D,\alpha}$ is not sufficient to represent the hysteretic features described in Sec. II, it provides a basic insight into the effects induced by the assumed or observed characteristics $\Delta p = q^{-1}(Q_V)$. However, these memoryless models are not capable of accurately representing the damper characteristics observed in Fig. 1. Therefore, the model shown in Eq. (7) will be considered further. The considerations related to equations $\Delta p = q^{-1}(Q_V)$ are applicable in this instance as well. In the case of Eq. (7), the volumetric fluid flow rate is symbolically written in the directional form $Q_V(\Delta p) = \text{sign}(\Delta p) Q_V(|\Delta p|)$. A possible practical implementation of the damper structure shown in Fig. 2 can be realized with controllable components based on the servo-valve architecture (e.g., [1,4–6]). The relationship between Q_V and Δp is again based on the considerations related to equations $\Delta p = q^{-1}(Q_V)$ [e.g., Eq. (9)]. The static characteristic of the valve is constituted by the algebraic relationship between these variables and a new variable $u(t) \in \mathbb{R}$ representing variation (e.g., displacement, rotation, etc.) of the controllable/active element of the valve. Based on the previous discussion, the relationship is assumed to be of the form $\Delta p = D_2 Q_V |Q_V|$, leading to the relationships $\Delta p = q^{-1}(Q_V)$ and $Q_V = q(\Delta p)$ (e.g., [33]) as follows:

$$\begin{aligned} \Delta p &= \{\rho/[2(C_D A_V)^2]\} Q_V |Q_V| \\ Q_V &= \text{sign}(\Delta p) C_D(\mathcal{U}) A_V[u(t)] \sqrt{(2/\rho)|\Delta p|} \\ &= \text{sign}(\Delta p) A_{PV}(\bar{u}) \sqrt{|\Delta p|} \end{aligned} \tag{10}$$

where variable

$$A_{PV}(\bar{u}) = C_D(\mathcal{U}) A_V[\overline{u} u_{\text{lim}}] \sqrt{(2/\rho)}$$

is the pseudosection function, $\mathcal{U} \in \{Re, \text{geom}, \dots\}$ is the set of all factors influencing the fluid flow through the restrictor [33], $\overline{u}(t)$ is the scaled form of $u(t)$, where $u(t) = \overline{u}(t) u_{\text{lim}}$ and u_{lim} is the limit change of the control variable. Static model(10) of the volumetric flow rates through a variable opening/valve, where Q_V is proportional to $\sqrt{|\Delta p|}$, is used in the hydraulic actuator modeling for the servo-valve models (e.g., [25–27]) and for the damper-related modeling activities (e.g., [4–6]). The effect of the members of the set $\mathcal{U}$ on varying C_D is particularly important for low fluid velocities, restricted flows, leak flows, and flows due to small Δp, as illustrated by Fig. 3. The concept of variable pseudosection parameter is also shown here in Fig. 3 [33].

The damper, as shown in Fig. 2, can be initially assumed in some reference configuration $A_{PV}(\bar{u}_{\text{ref}})$, where $0 < \bar{u}_{\min} < \bar{u}_{\text{ref}} < \overline{u}_{\max}$ with further activity limited such that $\overline{u}_{\min} \le \overline{u}(t) \le \overline{u}_{\max}$. Based on previous discussions, the model of the valve pressure losses is adopted with constant C_D leading to the reduced form of Eq. (10):

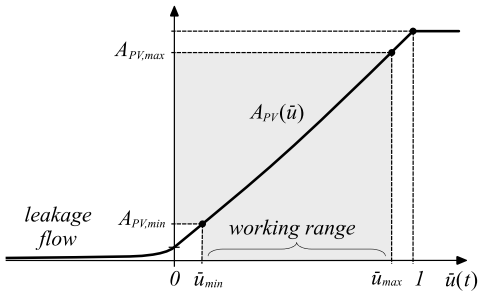

Fig. 3 Typical pseudosection function for a variable valve.

$$Q_V = \text{sign}(\Delta p) C_D A_V[u(t)] \sqrt{(2/\rho)|\Delta p|} \tag{11}$$

The model of the damper from Fig. 2 can be modified from Eq. (7), employing Eq. (11) to the following form:

$$\begin{aligned} \frac{\text{d}(\Delta p)}{\text{d}t} &= B_0 \left(\frac{1}{V_1(y_P)} + \frac{1}{V_2(y_P)} \right) \\ &\times \left\{ A_P \frac{\text{d}y_P}{\text{d}t} - \text{sign}(\Delta p) C_D A_V[u(t)] \sqrt{\left(\frac{2}{\rho}\right)|\Delta p|} \right\} \end{aligned} \tag{12}$$

This model of the damper provides information about the evolution of pressure differences Δp and therefore also about resulting damper forces. This is sufficient for present studies as the purpose of the research here is analysis of the physical mechanism behind perturbations of the standard damper behavior induced by parameter modulations. The damper model can be augmented by the model of the dynamics of active element. This model would introduce realistic response limitations with respect to any required active regime. Examples of relevant research can be found in papers [27,33].

Finally, it is instructive to relate this model to the work presented by Eyres [21]. If small oscillations around the reference piston position are assumed, the following relationship between initial volumes of the two working chambers can be written as $V_{02} = \lambda V_{01}$ (V_{01} and V_{02} are the constant initial volumes), $V_j[y_P(0)] = V_{0j}$ ($j = 1, 2$), and $\lambda = \mathbb{R}^+$. Adopting notation for the orifice flow rate $Q_O = Q_V$, general equation (7) can be rearranged to the form

$$\Delta \dot{p} = [(1 + \lambda)/\lambda \beta_0 V_{01}][A_P \dot{y}_P - Q_O(\Delta p)] \tag{13}$$

which can be further reduced assuming an initial central position of the symmetric damper with $\lambda = 1$:

$$\Delta \dot{p} = (2/\beta_0 V_{01})[A_P \dot{y}_P - Q_O(\Delta p)] \tag{14}$$

Equations (13) and (14) correspond to the hydraulic part of the model used for the model of the damper with relief valves investigated in [21].

IV. Semi-Active Damper Control Regimes

A. Semi-Active Mode of the Damper Model

Equations (7) and (12) represent a relatively complete model of the generic symmetric damper shown in Fig. 2, featuring a quadratic orifice and compressible fluid in steady thermal conditions. The external variation of the parameters related to the model of the valve influencing damper's behavior via characteristics $Q_V = q(\Delta p)$ can induce a semi-active mode of the damper operation. Introducing parametric control over the selected subset of the valve's physical parameters modifies the original static characteristics to the new parametric form $Q_V = q(\Delta p; \mathbf{p}_V)$, where $\mathbf{p}_V \in \mathbb{R}^{N_V}$ represents the vector of N_V physical valve parameters. Technically, the optimal choice of the parameter values $\mathbf{p}_V = \mathbf{p}_{V,\text{opt}}$, either in the local damper or an overall structural context, can be the subject of a broader optimization study based on the specifics of any future application.

The current problem specification assumes consideration of the time-variable parameters $\mathbf{p}_V(t)$ in the context of a periodic working environment. A set of all valve parameters is divided into the subset $\mathbf{p}_{V,S}$ of the constant parameters and the subset $\mathbf{p}_{V,A}(\psi)$ of the time-variable and periodic parameters, where $\psi \in [0, 2\pi]$ is the angular variable (azimuth angle) often used for the applications with rotating components, generally expressed as $\psi = \Omega t$, with Ω representing the nominal rotating frequency.

The previously introduced configuration leads to a new parametric formulation of the valve static characteristics:

$$Q_V = q[\Delta p; \mathbf{p}_{V,S}, \mathbf{p}_{V,A}(\psi)], \qquad \mathbf{p}_{V,A}(\psi) = \mathbf{p}_{V,A}(\psi + 2\pi) \tag{15}$$

Based on the formulation in Eq. (15), the damper model with a controllable or variable valve can be written as follows:

$$\frac{\mathrm{d}(\Delta p)}{\mathrm{d}t} = B_0\left(\frac{1}{V_1(y_P)} + \frac{1}{V_2(y_P)}\right) \times \left\{A_P \frac{\mathrm{d}y_P}{\mathrm{d}t} - Q_V[\Delta p;\, \mathbf{p}_{V,S},\, \mathbf{p}_{V,A}(\psi)]\right\}$$
$$F_D = A_P \Delta p \tag{16}$$

or in the general dynamic system terminology, the damper model has the following state-space form:

$$\dot{\mathbf{x}} = \mathbf{f}[\mathbf{x},\, \psi;\, \mathbf{p}_{V,S},\, \mathbf{p}_{V,A}(\psi)], \qquad \mathbf{x} \in \mathbb{R}^{N_D}$$
$$\psi \in \mathcal{D}_\psi \equiv [0,\, 2\pi], \qquad \mathbf{p}_{V,S} \in \mathbb{R}^{N_{V,S}}$$
$$\mathbf{p}_{V,A}(\psi) = \mathbf{p}_{V,A}(\psi + 2\pi) \in \mathbb{R}^{N_{V,A}} \tag{17}$$

where N_D is the number of damper model states and $N_V = N_{V,S} + N_{V,A}$ represents the division of all available valve performance parameters into the static (or constant) and the variable (or active) parameter subsets.

Model (17) is further used to produce derived response quantities (in the current investigation, a single damper force) thus establishing a direct link between the valve activity and the damper force output:

$$r \equiv F_D = g[\mathbf{x};\, \mathbf{p}_{V,S},\, \mathbf{p}_{V,A}(\psi)] \in \mathbb{R} \tag{18}$$

where r is the output response and $g(\circ)$ represents the general nonlinear response-generating function used for performance evaluations and the physical integration into wider structural contexts (e.g., coupled structural analyses).

B. Parameterization of the Damper Activity Signal

The semi-active control regime with the use of the semi-active damper is based on the assumption of effective parameter activity described by relationships (15) and (16) or, in general, Eq. (17). This effect translates into the output response quantities, as shown in Eqs. (16) or (18). The parameter activity is represented by the vector subset $\mathbf{p}_{V,A}(\psi)$. For the parameter activity to be acceptable within a given computational and operational framework, the $2\pi/\Omega$-periodicity is assumed, such that $\mathbf{p}_{V,A}(\psi) = \mathbf{p}_{V,A}(\psi + 2\pi)$ and $d\mathbf{p}_{V,A}(0)/d\psi = d\mathbf{p}_{V,A}(2\pi)/d\psi$.

The physical parameter activity parameterization introduces a second layer of the parameterization of the problem and it also establishes a control signal family $\mathcal{P}$. This layer of the parameterization enables further analytical and numeric handling of the problem. The definition of the activity parameterization

$$\mathbf{p}_{V,A} = \mathbf{p}_{V,A}(\psi; \mathbf{p}) \tag{19}$$

where $\mathbf{p} \in \mathbb{R}^{N_P}$ is the (realization of) parameterization of the control signal family $\mathcal{P}$. It introduces new parametric relationships by its propagation into the associated component characteristics and the state-space equations:

$$Q_V = q[\Delta p;\, \mathbf{p}_{V,S},\, \mathbf{p}_{V,A}(\psi;\, \mathbf{p})] \tag{20}$$

$$\dot{\mathbf{x}} = \mathbf{f}[\mathbf{x},\, \psi;\, \mathbf{p}_{V,S},\, \mathbf{p}_{V,A}(\psi;\, \mathbf{p})] \tag{21}$$

The concept of activity parameterization based on the two specific signal families $\mathcal{P}$ will be introduced and demonstrated in the following sections.

1. *Piecewise Polynomial-Periodic Damper Activity Parameterization*

One possible control signal family $\mathcal{P}_\chi$ satisfying previous requirements can be based on the sequence of the piecewise polynomials $\chi_j(\psi)$, defined locally such that $\psi \in \mathcal{D}_j \subset [0, 2\pi]$, establishing suitable activity parameterization of the elements of the vector $\mathbf{p}_{V,A}(\psi)$. A single active parameter $p_{V,A,i}(\psi)$ can be assumed in the following form:

$$p_{V,A,i}(\psi) = p_{V,A,i,0}\left[1 + \bigcup_{j=1}^{N_I} \chi_j(\mathcal{D}_j)\right] \tag{22}$$

where $p_{V,A,i,0} \neq 0$ is the nominal, reference, or initial parameter value, N_I is the total number of the intervals $\mathcal{D}_j$, and $\chi_j(\psi)$ is defined such that

$$\mathcal{D}_\psi = \bigcup_{j=1}^{N_I} \mathcal{D}_j = [0,\, 2\pi], \quad \mathcal{D}_k \cap \mathcal{D}_l = \emptyset \quad \forall\, k,\, l\colon k \neq l \tag{23}$$

Control segment $\chi_j(\mathcal{D}_j)$ is defined on its local domain $\mathcal{D}_j = [\psi_j, \psi_{j+1}]$ as the zero-slope control-point cubic polynomial with the local coordinate system $\bar{\psi} = [0, 1]$:

$$\chi_j(\bar{\psi}) = \sum_{m=0}^{3} a_{j,m} \bar{\psi}^m, \qquad \bar{\psi} = \frac{(\psi - \psi_j)}{(\psi_{j+1} - \psi_j)} \tag{24}$$

where the four coefficients $a_{j,m}$ are assumed to be specified so the following continuity conditions are satisfied:

$$\chi_j'(0) = \chi_j'(1) = 0, \qquad \chi_{j-1}(1) = \chi_j(0) = p_j$$
$$\chi_j(1) = \chi_{j+1}(0) = p_{j+1}, \qquad \bigcup_{(j)} [\psi_j,\, \psi_{j+1}] = [0,\, 2\pi]$$
$$\mathcal{D}_k \cap \mathcal{D}_l = \emptyset, \quad \forall\, k,\, l\colon k \neq l \tag{25}$$

A set of the cubic piecewise polynomials $\chi_j(\mathcal{D}_j)$ is thus used according to Eqs. (24) and (25), resulting into the signal (waveform) representing the parameter activity $p_{V,A,i}(\psi)$, see Eq. (22). Specific cubic polynomial parameterization (24) and (25) is chosen as a convenient, continuous, and periodic time-domain signal representation suitable for later practical use. A set of the parameters defined via the condition $\chi_{j-1}(1) = \chi_j(0) = p_j$ and associated continuity conditions constitutes an activity parameterization with the parameter vector $\mathbf{p} = [p_j] \in \mathbb{R}^{N_P}$ uniquely specifying the active signal waveform, where N_P represents the number of the parameters in the activity parameterization. In this case, parameters p_j directly represent the waveform's control points, as will be also shown later in the second case study of this paper.

2. *Multiharmonic Parameterization of Damper Activity*

This section deals with another form of activity parameterization that is specifically suited for application in periodically operating structures or machinery. Based on the nature of the current application, the multiharmonic control signal family $\mathcal{P}_{\mathrm{HHC}}$, often used in the field of HHC, can be chosen. The sum of the harmonic members constituting the family $\mathcal{P}_{\mathrm{HHC}}$ with their frequencies defined as integer multiples of the Ω can be written either in the absolute form

$$p_{V,A,i}(\psi) = p_{i,0} + \sum_{k=1}^{N_P/2} [p_{i,C,k} \cos(k\psi) + p_{i,S,k} \sin(k\psi)]$$
$$\mathbf{p} = [p_{i,C,k},\, p_{i,S,k}] = [p_{i,C,1},\, p_{i,S,1},\, \ldots,\, p_{i,C,N_P/2},\, p_{i,S,N_P/2}] \in \mathbb{R}^{N_P} \tag{26}$$

or in the normalized form:

$$\bar{p}_{V,A,i}(\psi) = 1 + \sum_{k=1}^{N_P/2} [\bar{p}_{i,C,k} \cos(k\psi) + \bar{p}_{i,S,k} \sin(k\psi)]$$
$$\mathbf{p} = [\bar{p}_{i,C,k},\, \bar{p}_{i,S,k}] = [\bar{p}_{i,C,1},\, \bar{p}_{i,S,1},\, \ldots,\, \bar{p}_{i,C,N_P/2},\, \bar{p}_{i,S,N_P/2}] \in \mathbb{R}^{N_P} \tag{27}$$

assuming that $p_{i,0} \neq 0$, $\bar{p}_{i,C,k} = p_{i,C,k}/p_{i,0}$, and $\bar{p}_{i,S,k} = p_{i,S,k}/p_{i,0}$. The physical value of the parameter will then be regained from the relationship $p_{V,A,i}(\psi) = p_{i,0}\bar{p}_{V,A,i}(\psi)$.

Alternatively, an equivalent to sine–cosine forms (26) and (27), the amplitude-phase form can be employed for the jth pair of the single

harmonics via the correspondence $\{\bar{p}_{i,C,j},\ \bar{p}_{i,S,j}\} \rightarrow \{\bar{A}_{i,j},\ \phi_{i,j}\}$, where $\bar{A}_{i,j} = \sqrt{\bar{p}^2_{i,C,j} + \bar{p}^2_{i,S,j}}$ and $\tan(\phi_{i,j}) = \bar{p}_{i,S,j}/\bar{p}_{i,C,j}$. Both multiharmonic representations of the activity parameterization will be used in this paper.

V. Case Studies

A. Demonstration of the Compressibility Effects in the Quadratic Flow Restrictor

The qualitative nature of the model described by Eq. (12) and Fig. 2 is demonstrated for the case with $\beta_0 = 1/B_0 \neq 0$ and the harmonic piston excitation $y_P(t) = Y_P \sin(2\pi f_P t)$. A simple fixed circular orifice is assumed with $A_V = \pi d_O^2/4$. Figure 4 demonstrates the scaled responses of three different damper configurations in the velocity-force domain. The case with the maximum response, Fig. 4a, is scaled with respect to its maximum force during one steady cycle. Piston displacement $y_P(t)$ is retained identically for all three cases. The remaining two cases, Figs. 4b and 4c, are scaled relatively to the case in Fig. 4a. The compressibility coefficients are $\beta \in \{\beta_0,\ 10\beta_0,\ 50\beta_0\}$.

The quadratic nature of the damper is observable in all subplots, particularly in Fig. 4a. Increasing the compressibility causes a smoother response; increasing lag between the piston excitation and the damper force response manifests itself in the form of increasing hysteresis in the velocity-force domain, and it also produces a reduced response maxima for increased β. To complement this demonstration, Fig. 5 shows similar effects of increased hysteresis in the velocity-force domain for a constant β and changing diameter of the orifice d_O. The applied piston excitation is identical to the one used in the previous case. Furthermore, scaling is applied here with respect to the maximum force response from Fig. 5c.

Decreasing the size of the orifice causes not only an increase in the forces generated by the damper for the identical excitation scenario, but it also promotes an increased hysteretic behavior due to the increased participation of the compressibility term in the flow rate equilibrium within the fluid volume. Figure 5 also illustrates a basic philosophy behind the concept of a semi-active damper in which the form of the damper response for given conditions can be altered by a change of the physical parameter from Eq. (12) or, more specifically, from the flow rate Q_V.

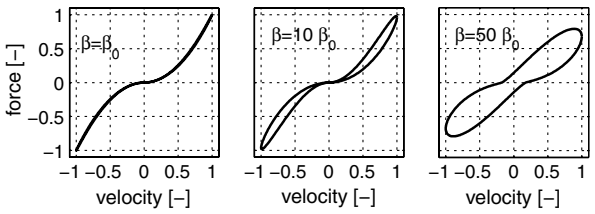

Fig. 4 The effect of compressibility on velocity-force characteristics of a damper with a compressible fluid (scaled with respect to maximum components of Fig. 4a).

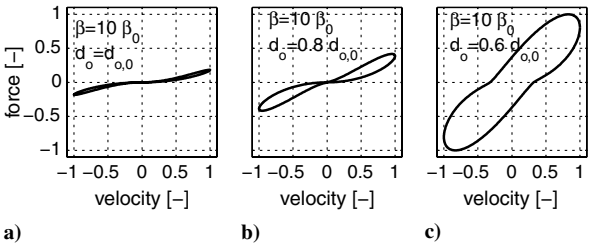

Fig. 5 The effect of orifice variation on velocity-force characteristics of a damper with a compressible fluid (scaled with respect to maximum components of Fig. 5c).

B. Demonstration of Periodic Valve Perturbation and its Effect on the Damper Behavior

This case study focuses on the analysis of specific physical mechanisms resulting from the periodic parameter modulation. The qualitative nature of previous developments is demonstrated in this section via the case of the damper represented by Eq. (16) with valve characteristics according to Eq. (11) and the periodic parameter modulation of the opening similar to the traditional servo-valve designs. Based on the discussion provided in Sec. III, the valve characteristics are assumed in the following simplified form:

$$\begin{aligned} Q_V(\Delta p,\ \psi) &= \operatorname{sign}(\Delta p) C_D b_V x_V(\psi) \sqrt{(2/\rho)|\Delta p|} \\ &= \operatorname{sign}(\Delta p) K x_V(\psi) \sqrt{|\Delta p|}, \\ x_V(\psi) &\equiv u(\psi) = u(\psi + 2\pi) \end{aligned} \tag{28}$$

where the parameter vectors listed in Eq. (15) are defined as $\mathbf{p}_{V,S} = [C_D(\mathcal{U}),\ b_V]^T$ and $\mathbf{p}_{V,A}(\psi) = [x_V(\psi)]$. The previous definition leads to system (16) with the input set $\mathcal{I} \in \{\dot{y}_P,\ x_V\}$ and the output set $\mathcal{R} \in \{F_D\}$.

A simple perturbation $\Delta x_{V,\text{ptb}}$ to the nominal signal $x_V(\psi) = x_{V,0}$ is assumed to be applied periodically with a fundamental period $2\pi/\Omega$, as indicated in Fig. 6. This form of periodic damper activity is used as it facilitates the analysis of the physical mechanisms in action due to its time-localized nature. Each transition between the nominal and the perturbed level lasts δ_{ptb} and is realized by the third-order C^1-smooth polynomial function. The perturbed level itself lasts $\Delta\psi_{\text{ptb}}$. This signal form represents a single periodic event within its domain. In addition to this form of periodic valve perturbation, an alternative harmonic modulation will be demonstrated later in this paper.

The activity function $x_V(\psi)$ is analytically implemented as a piecewise C^1-smooth union of N_I normalized control functions χ_j defined in their respective domains $\mathcal{D}_j$ such that

$$x_V(\psi) = x_{V,0}\left[1 + \bigcup_{j=1}^{N_I} \chi_j(\mathcal{D}_j)\right] \tag{29}$$

where $x_{V,0}$ is the reference physical value of the valve opening. The remaining properties of this activity parameterization are defined in accordance with the specification provided in Sec. IV.

The specification of the valve activity, according to Eq. (29), leads to a defined activity parameterization. The bounding points of the chosen intervals establish a set of the control points that also provides activity parameters for a given definition. The current parameterization is designed as described in Table 1. The physical values of the damper model [see Eq. (16)] parameters are specified in Table 2.

Sine excitation of the damper piston is chosen in the form $y_P(\psi) = Y_P \sin(\psi)$ with amplitude $Y_P = 0.01$ m and a frequency of excitation $f_P = 3.0$ Hz, assuming $\psi = 2\pi f_P t$. The two inputs to the system specified by Eq. (16) are $\dot{y}_P(\psi)$ and $x_V(\psi)$, and the observed output is $F_D(\psi)$, approximately proportional to $\Delta p(\psi)$ and evolving according to Eq. (16). Apart from these quantities, due to the physical nature of the model, it is possible to observe internal derived variables such as the flow rates associated with different subcomponents of the damper. Based on the form of Eq. (16), three volumetric flow rates will be observed:

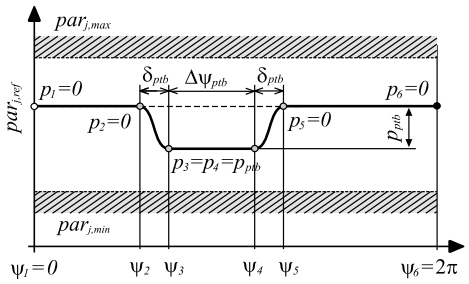

Fig. 6 Example of a valve activity with a fundamental period of 2π.

Table 1 Parameterization specification for activity demonstration

	Control point no. (ID)					
	1 (-)	2 (A)	3 (B)	4 (C)	5 (D)	6 (-)
Azimuth position, deg	0	45	75	105	135	360
Perturbation, %	0	0	−75	−75	0	0

Table 2 Nominal parameters used in the damper study with periodic perturbation

Parameter name, units	Parameter label	Parameter value
Fluid compressibility, Pa^{-1}	$\beta_0 = 1/B_0$	1.39e − 9
Reference volume of chamber, m^3	V_0	3e − 4
Flow discharge coefficient	C_D	0.6500
Opening width, m	b_V	0.0050
Opening length (reference), m	$x_{V,0}$	0.0019
Fluid dynamic viscosity, Pa · s	η	0.0300
Piston cross section, m^2	A_P	0.0035
Fluid density, kg/m^3	ρ_0	820.0000
Orifice length, m	l_O	0.0010

$$Q_\beta(\psi) = \mathcal{K}[y_P(\psi)]\Delta\dot{p}(\psi)$$

where

$$\mathcal{K}(y_P) = \beta_0 V_1 V_2/(V_1 + V_2), \qquad V_j = V_j(y_P)$$

$Q_V(\psi)$ and $Q_P(\psi) = A_P\dot{y}_P(\psi)$. A balance of these quantities represents a fundamental concept in the construction of model (16). Two representations of the damper working cycle shown here are the damper force-velocity and force-displacement characteristics, indicating the hysteretic effects and work done during one cycle W_{PC}, respectively. The Fourier analysis of the damper output $F_D(\psi)$ for inactive and semi-active regime is presented, demonstrating the central idea of the active components in the flow-metering regime: the output frequency and the phase induced and modified by the use of an active component.

For the numeric computations, a suite of MATLAB®-based routines was programmed using the standard ordinary differential equation solver capabilities provided in this software environment [34]. Periodic regimes were simulated by allowing a suitable number of the cycles to stabilize the model to produce periodic responses. Typically, fewer then 10 cycles were sufficient to achieve this state.

The input–output relationship for the damper in a semi-active regime, according to Eq. (29) and Table 1, is shown in Fig. 7. The output damper force $F_D(\psi)$ is shown in physical units, and the input quantities located in the same graph are scaled accordingly to provide a suitable visual correlation between participating quantities. The reference inactive regime is denoted by the dashed lines, whereas the semi-active regime is indicated by the solid lines. Specific quantities are identified by corresponding labels placed directly in the figure.

The region of localized activity was selected to be located in the region with minimum velocities to indicate the velocity-sensitive nature of the damper operation and the capability of the parameter variation to induce significant response modifications while still respecting the damper's operational principles (e.g., of producing only motion-resisting forces.) The sectors A–B and C–D feature prespecified transitions to and from the perturbed state of the damper, whereas the sector B–C presents the locally perturbed region itself.

The previous results can be made more informative by plotting single parametric lines in the force-velocity $[\dot{y}_P(\psi),\ F_D(\psi)]$ and force-displacement $[y_P(\psi),\ F_D(\psi)]$ domains, as shown in Fig. 8. Again, the dashed lines indicate the reference inactive regime and the solid lines represent the semi-active regime as specified previously.

Both subplots indicate significant variation of the reference shapes due to parameter activity. In the force-displacement domain, an increase in W_{PC} is observed in the form of an increased area enclosed by the response line. In the force-velocity domain, the original quadraticlike loop is altered, producing a significant area enclosed by the corresponding response line. The increase in W_{PC} is related to the increasingly restrictive nature of the opening with its decreasing area, thus increasing hydraulic resistance to the fluid flow. To retain the balance between demanded and allowed flow rates, a compressible fluid compensates for reduced and increasingly restricted valve flow rates $Q_V(\psi)$ by inducing increased hysteresis to the system behavior. This is represented in the force-velocity domain as an increased area enclosed by the response line. This effect is more clearly demonstrated in Fig. 9, specifically by the evolution of $Q_\beta(\psi)$.

A detailed observation of the effects due to parameter activity is facilitated by the azimuth-dependent relationships of the relevant flow rate elements shown in Fig. 9. The top subplot of the figure shows a flow balance representation, and the bottom subplot presents the state variable $\Delta p(\psi)$ that is computed as the primary variable in the problem solution. Flow rates are labeled accordingly, directly in the figure. Index label 0 represents the reference operational regime and ptb denotes the regime with perturbed parameter activity.

The periodic perturbation event consists of the opening size reduction followed by a brief operation on the perturbed level and then a progressive return to the nominal value. It induces changes in the flow rate ratios while the flow rate balance $Q_\beta(\psi) + Q_V(\psi) +$

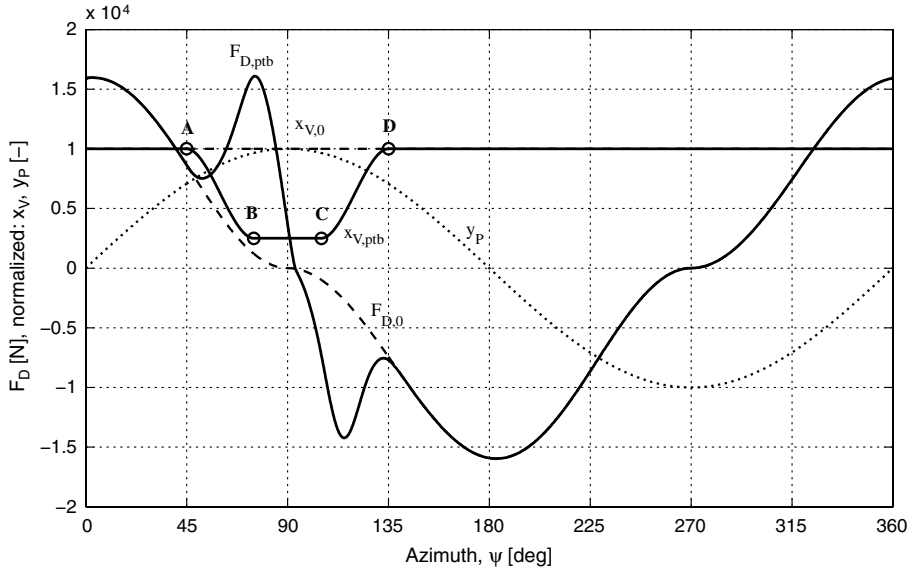

Fig. 7 Operation of a semi-active damper with a locally perturbed control input.

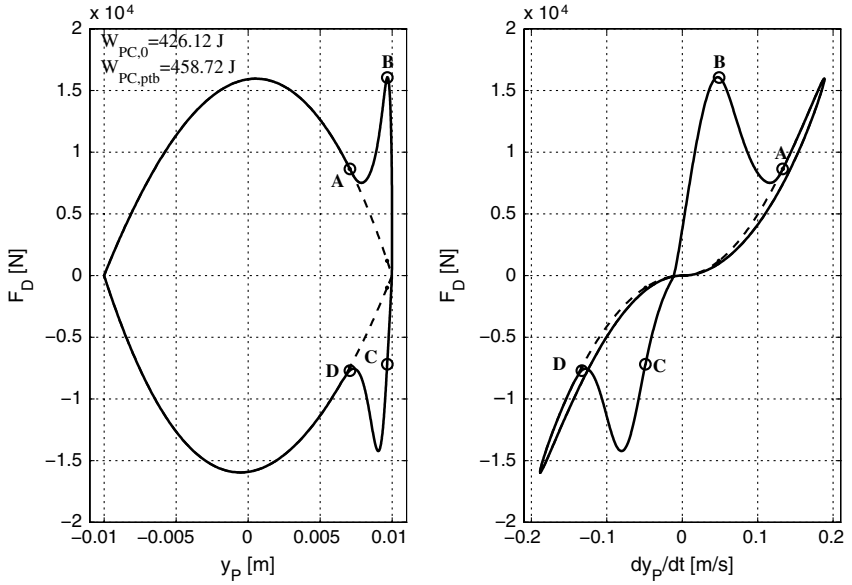

Fig. 8 Operation of a perturbed semi-active damper in force-displacement and force-velocity domains.

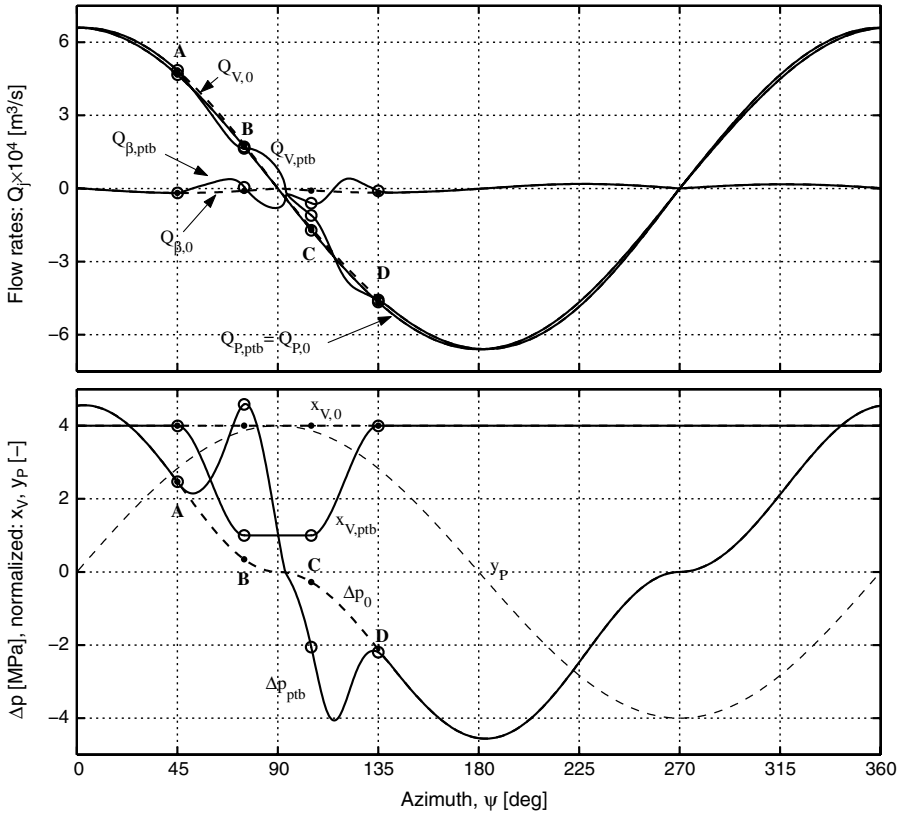

Fig. 9 Flow rate balances and differential pressure in a semi-active damper due to periodic piston excitation and valve perturbation.

$Q_P(\psi) = 0$ is always retained. In this specific case, the decrease in $x_V(\psi)$ after the point A induces increased participation of $Q_\beta(\psi)$; this also leads to the increase in the pressure difference $\Delta p(\psi)$ peaking at the point B. In the meantime, the second input parameter $\dot{y}_P(\psi)$ decreases to 0, as observed in Fig. 9, via a reduced slope of $y_P(\psi)$ for $\psi \to 90$ deg. This allows a reduction of the high Δp after point B via an increased participation of $Q_V(\psi)$. The changes of $Q_\beta(\psi)$ are directly linked with the evolution of the state variable Δp via $Q_\beta(\psi) \sim \Delta\dot{p}(\psi)$, where Q_β can be thought of as the combination of its chamber constituents $Q_\beta = \mathcal{K}(\dot{p}_1 - \dot{p}_2) = Q_{\beta,1} - Q_{\beta,2}$. Therefore, the compressibility-induced volumetric flow rate $Q_\beta(\psi)$ itself represents the balance between the corresponding compressibility flow rate changes in the separate chambers.

The character of $\Delta p(\psi)$ also indicates the extent of the hysteretic behavior of the system. This can be observed by comparing $\Delta p_0(\psi)$ and $\Delta p_{\text{ptb}}(\psi)$. The regime with the static opening responds to $\dot{y}_P \to 0$ almost immediately. In the perturbed system, when $\dot{y}_P = 0$ and $Q_P = A_P\dot{y}_P = 0$, the flow equilibrium condition is $Q_\beta + Q_V = 0$, whereas the flows Q_β and Q_V remain relatively largely perturbed. This leads to a delayed decreasing $\Delta p \to 0$ in the effort to achieve instantaneous pressure equilibrium. Therefore, the time instant with $\Delta p = 0$ is lagging after the specific event that causes this

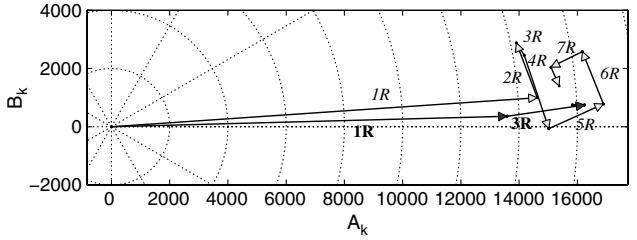

Fig. 10 Fourier analysis of nominal and perturbed damper force waveforms (dark arrows and bold font indicate nominal regimes and light arrows and italic font denote semi-active regimes).

effect in the incompressible setting. The degree to which this lagging effect occurs can be attributed to the combinations of the inputs to the system; in this case, $\dot{y}_P$ and x_V. This lagging behavior shows in the velocity-force domain as perceived hysteresis.

The effect demonstrated in Fig. 7 (i.e., the alteration of the damper response from $F_{D,0}(\psi)$ to $F_{D,\mathrm{ptb}}(\psi)$ due to modulated parameter $x_V(\psi)$ for given velocity profile $\dot{y}_P(\psi)$ in the periodic operational regime) can be further analyzed in the frequency domain. Fourier analysis of the periodic nominal $F_{D,0}(\psi)$ and the modulated $F_{D,\mathrm{ptb}}(\psi)$ is presented in Fig. 10 in the form of an Argand diagram. The separate frequency components in the figure are denoted as xR and $x = 1, 2, \ldots$, where x denotes the integer multiple of the fundamental angular frequency Ω of the rotating component.

By providing information about the phase and the magnitude, Fig. 10 allows observation of the influence of the periodic parameter modulation on the response content in the frequency domain. Figure 10 indicates that the use of the periodic parameter modulation, such as the dimensional variation of the passage between the two working chambers of the damper, can be used to alter the magnitudes and the relative phases of the response's frequency components. As an example, in the current case, the chosen parameter type and its associated periodic waveform induced significant increase in the magnitude of $2R$ and the reduction and phase change of the $3R$ component of $F_{D,\mathrm{ptb}}(\psi)$. Further interest can therefore be directed toward establishing a theoretical and computational framework in which these effects could be employed advantageously in the

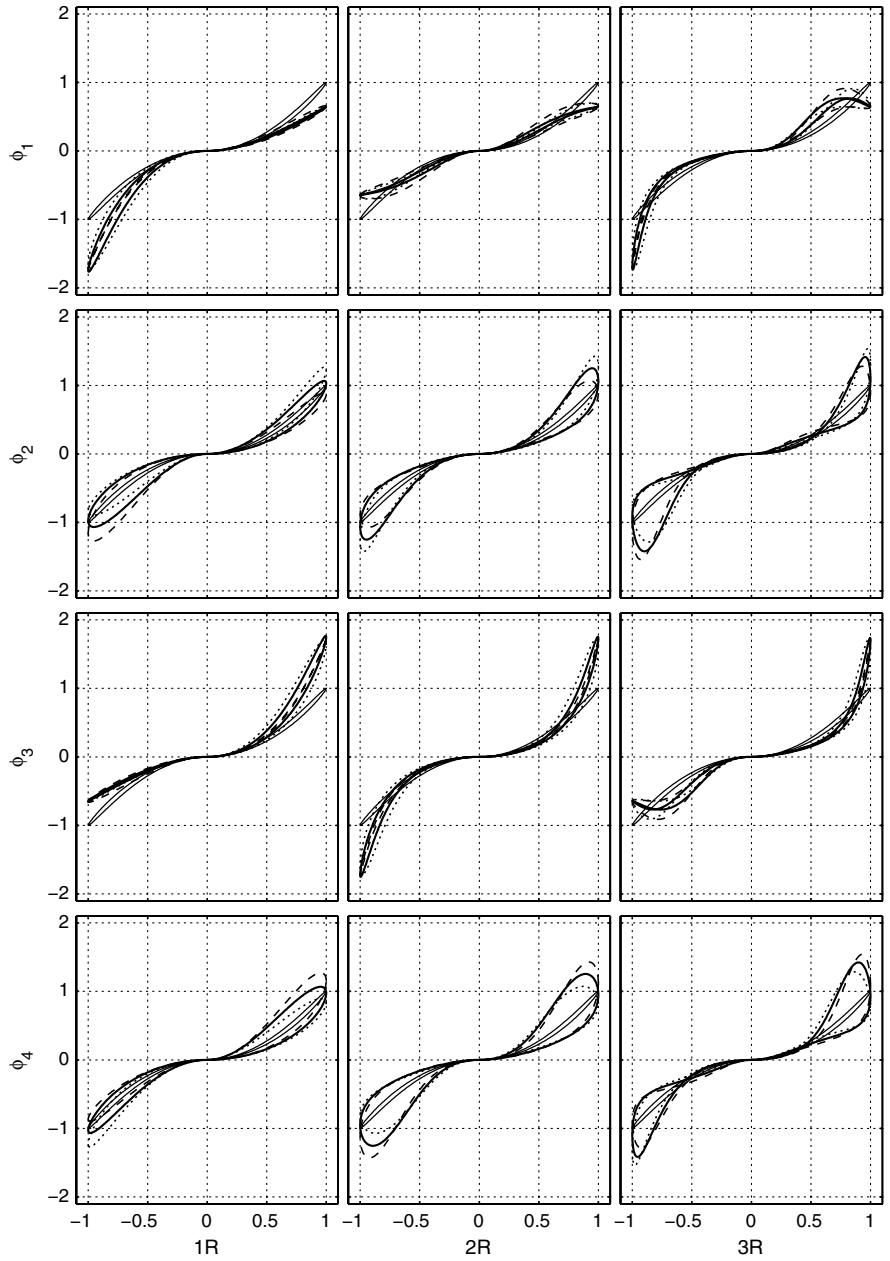

Fig. 11 Force-velocity domain of the semi-active damper with reference piston input, harmonic damper activity with changing frequencies (columns), and phases (rows) (scaled with respect to a nominal scenario).

periodic modulation-based semi-active vibration control of periodically operating systems. This can be achieved in rotating systems in which only certain harmonic force components filter from the rotating coordinates system to the fixed frame, and thus the periodic modulation can be focused on the modifications of only selected frequency components of the responses in the rotating coordinate frame.

C. Demonstration of Harmonic Modulation of the Damper Parameter

The identical computational configuration to that specified in the previous section will be used in this section to present a demonstration of single harmonic damper activity with the fixed reference piston excitation. The piston excitation is identical to that presented previously. Parameter activity will be conveniently described as single harmonics with phase delay in the normalized form:

$$x_V(\psi) = x_{V,\text{mean}}[1 + \bar{X}_V \cos(k\psi + \phi_X/k)] \tag{30}$$

where the normalized amplitude of the harmonics $\bar{X}_V$ and its phase shift ϕ_X will be defined differently for different studies. Parameterization of the activity signal in this case is therefore $\mathbf{p} = [\bar{X}_V, \phi_X]$. The value of the mean or the reference opening $x_{V,\text{mean}}$ is the same as the previous case study. In the parametric studies presented here, the normalized amplitude of the harmonic variation is $\bar{X}_V = 0.25$.

Two parametric studies are provided in this section to demonstrate the effect of the harmonic parameter activity. In the first study, harmonic frequencies kR and phase shifts ϕ_X for given $\bar{X}_V$ will be used to provide the force-velocity and the force-displacement characteristics. In the second study, a single harmonics will be investigated for the full range of the phase shifts $\phi_X \in [0, 2\pi]$.

The first parametric study is presented in Figs. 11 and 12. Figure 11 demonstrates the force-velocity domain of the activated damper, whereas Fig. 12 presents results in the force-displacement domain. In both figures, the columns correspond to the frequencies $\{1, 2, 3\}R$ and the rows correspond to the varying phase shifts

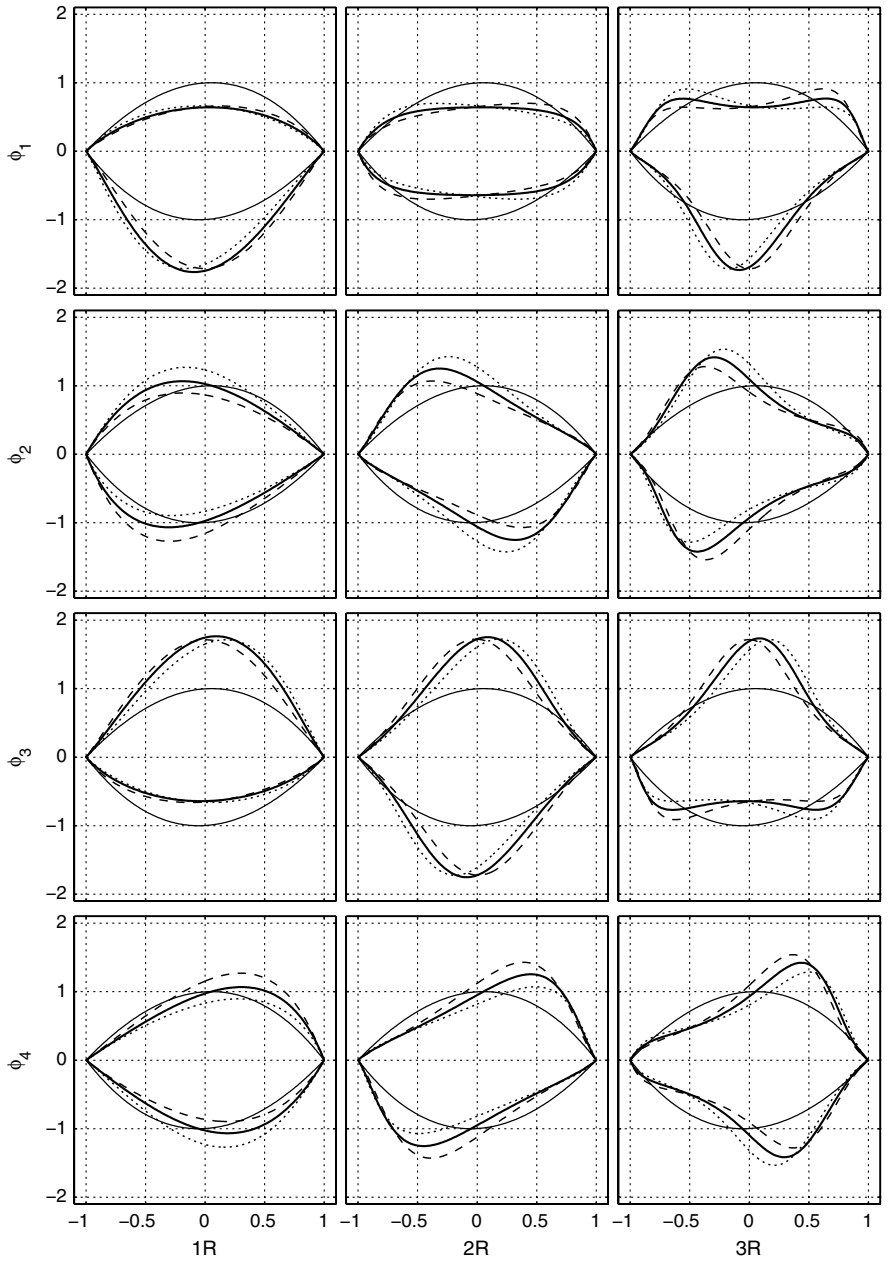

Fig. 12 Force-displacement domain of the semi-active damper with reference piston input, harmonic damper activity with changing frequencies (columns), and phases (rows) (scaled with respect to a nominal scenario).

$\phi_X \in \{0, 90, 180, 270\}$ deg. Angle ϕ_X/k is the actual relative phase angle between the signal $x_V(\psi)$ with frequency $f_{P,k} = kf_P$ and the signal $y_P(\psi)$ with frequency f_P. Moreover, main shifts are complemented with a pair of responses generated only for the shifts $\phi_X \pm \Delta\phi_X$, where $\Delta\phi_X = 20$ deg to indicate variability associated with the parameter change. Within both figures, reference results are presented by the thin solid lines, whereas thick solid lines demonstrate the specific main cases of the parameter pairs $[\bar{X}_{V,r}, \phi_{X,s}]$. Dotted lines denote the cases corresponding to $\phi_X + \Delta\phi_X$ and the dashed lines denote cases $\phi_X - \Delta\phi_X$. All results are scaled with respect to the maximum absolute forces and the displacements derived from the reference case of the classical damper without parametric activity. The subplots are identically scaled to allow cross comparison of the results.

Obtained periodic solutions in both domains $[\dot{y}_P, F_D]$ and $[y_P, F_D]$ indicate that the application of the harmonic, or possibly multiharmonic, signals to describe the damper parameter activity in the periodic environment can lead to significant alterations of the reference characteristics. In the force-velocity domain, this is characterized by both increased and decreased effect of compressibility and associated delay, resulting in significant increases in the peak forces produced by the damper throughout the cycle. In the force-displacement domain, the area enclosed by the characteristic lines shows both effects: the increase and decrease of the work done per cycle; all this is dependent on a given configuration, the piston excitation frequency content, as well as the activity characterization in terms of the frequencies and the phase delays.

Previous results show that a semi-active damper in the periodic regime can induce both types of effects: for example, the effects with significantly increased resistance to provided motion due to temporal coincidence in high velocities and smaller valve openings or decreased resistance due to coincidence in the low piston velocity and increasing opening of the control valve. The effects associated with increased resistance and the damping capacity may result into high peak forces, and it is therefore expected that the choice of the parameter activity values in the semi-active damper will have to be augmented with a constraint limiting maximum allowable value of these forces.

The damper operation in assumed periodic conditions is now analyzed further, with the parameter activity frequency set at $3R$ and the full range of phase shifts $\phi_X \in [0, 2\pi]$. Figure 13 summarizes results of this study. It represents the Argand diagram for a number of damper force responses $F_D(\psi)$. Every closed loop within this figure is associated with a single frequency of the Fourier decomposition of $F_D(\psi)$. Furthermore, every point of these lines corresponds to the specific scenario with the activity amplitude $\bar{X}_V = 0.25$, the activity frequency $3R$, and a specific ϕ_X from the interval $[0, 2\pi]$. In total, 30 points ϕ_X were used from the interval with equidistant spacing constituting closed loops in the Argand domain of cosine and sine harmonic components of $F_D(\psi)$. In Fig. 13, harmonic components $\{2, 3, \ldots, 8\}R$ are shown. The loop corresponding to $1R$ is not shown as it is displaced from the central part of the applied axes boundaries. The $1R$ component is the dominant harmonic component of $F_D(\psi)$, as shown in Fig. 7, and also indicated for a single case in Fig. 10. Moreover, this quantity does not indicate significant variability while varying ϕ_X. Figure 13 uses physical units of the damper force F_D.

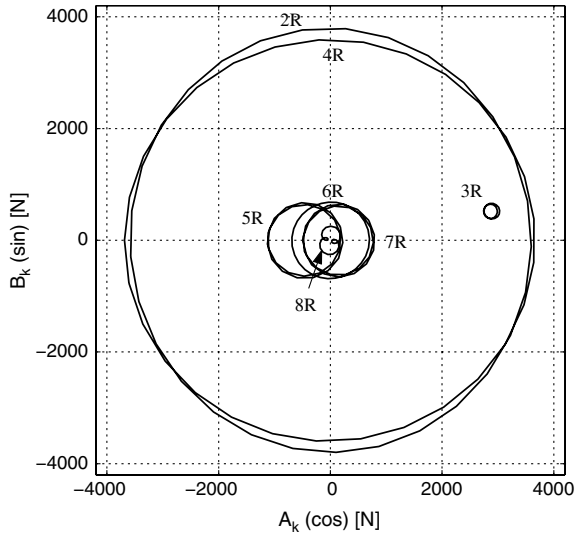

Fig. 13 Harmonic representation of the damper forces in the parametric study with parameter activity based on $3R$ harmonic variation with the full range of phase delays.

This figure gives closer insight into the effects of the internal damper parameter modulation/activity for the specified piston excitation scenario. The size of the closed loops is indicative of the sensitivity of the frequency components of F_D with respect to the parameter changes. Figure 13 clearly indicates dominance of the $2R$ and $4R$ response alterations induced by the $3R$ parameter activity for the full range of the phase shifts $\phi_X \in [0, 2\pi]$. This observation suggests a possible mechanism relating the interaction of the two inputs $\dot{y}_P$ and x_V on the single observed response F_D within the context of the studied nonlinear system [e.g., Eq. (16)]. In the current scenario, the dominant input frequency components from both input sources (i.e., the piston oscillation at $1R$ and the parameter modulation at $3R$) couple together so that the major influence on F_D is observed at one-multiple $4R$ and half-multiple $2R$. It is this effect of mutual frequency-based coupling leading to the ability of multifrequency phasing that can be further developed in the complete computational framework, including a semi-active damper as its subcomponent.

VI. Conclusions

This paper introduces analysis of a semi-active hydraulic damper in a periodic working environment. This assumption, in the broader sense, establishes an instance of a semi-active vibration controlling device. The two principal theoretical aspects of this paper are the application of standard hydraulic system theory considerations and assumed periodic damper excitation along with imposed periodic damper modulation. The damper modulation is implemented via two alternative approaches: local parameterization using a piecewise polynomial representation and global parameterization using a multiharmonic representation of damper modulation signal.

Assuming a discrete frequency content based on the identical fundamental frequency, the periodic modulation mode of the semi-active device in the periodic working environment is assumed to retain the periodic nature of the responses of the interest in the steady (e.g., trimmed) modes of operation. The semi-active device presented in this paper is a hydraulic damper with a controlled flow restrictor between the two working chambers of the damper. This provides a realistic, robust, and practical platform of general utility in semi-active control in assumed operating conditions. A controlled flow restrictor induces changes in the generalized flow rate balance equation, including the effect of the fluid compressibility that is a characteristic factor of these systems. The physical reasons behind the damper response modulation are described and explained in the simulated case study of the damper with a realistic representation of the flow restrictor and other model parameters. This and the subsequent case study demonstrate that the assumed configuration of the damper can alter the response frequency content via internal periodic modulation of the physical parameters for given reference piston excitation conditions.

Based on the presented results, further considerations and development of this concept require 1) an integration of the damper into an application within which the damper could be used as semi-active vibration controlling device, and 2) further component-specific and application-specific sensitivity and performance studies of the internal mechanisms of the physical coupling between the structural excitation of the damper and the semi-actively induced flow modulations.

References

[1] Karnopp, D., "Design Principles for Vibration Control Systems Using Semi-Active Dampers," *Journal of Dynamic Systems, Measurement, and Control*, Vol. 112, No. 3, Sept. 1990, pp. 448–455. doi:10.1115/1.2896163

[2] Heo, S.-J., Park, K., and Son, S.-H., "Modelling of Continuously Variable Damper for Design of Semi-Active Suspension Systems," *International Journal of Vehicle Design*, Vol. 31, No. 1, 2003, pp. 41–57. doi:10.1504/IJVD.2003.002046

[3] Vahdati, N., and Ahmadian, M., "Variable Volumetric Stiffness Fluid Mount Design," *Shock and Vibration*, Vol. 11, No. 1, Jan. 2004, pp. 21–32.

[4] Patten, W. N., Sack, R. L., and He, Q., "Controlled Semiactive Hydraulic Vibration Absorber for Bridges," *Journal of Structural Engineering*, Vol. 122, No. 2, Feb. 1996, pp. 187–192. doi:10.1061/(ASCE)0733-9445(1996)122:2(187)

[5] Patten, W. N., Mo, C., Kuehn, J., and Lee, J., "A Primer on Design of Semiactive Vibration Absorbers (SAVA)," *Journal of Engineering Mechanics*, Vol. 124, No. 1, Jan. 1998, pp. 61–68. doi:10.1061/(ASCE)0733-9399(1998)124:1(61)

[6] Symans, M. D., and Constantinou, M. C., "Experimental Testing and Analytical Modelling of Semi-Active Fluid Dampers for Seismic Protection," *Journal of Intelligent Material Systems and Structures*, Vol. 8, No. 8, Aug. 1997, pp. 644–657. doi: 10.1177/1045389X9700800802

[7] Dugundji, J., and Wendell, J. H., "Some Analysis Methods for Rotating Systems with Periodic Coefficients," *AIAA Journal*, Vol. 21, No. 6, June 1983, pp. 890–897. doi:10.2514/3.8167

[8] Wereley, N. M., "Analysis and Control of Linear Periodically Time Varying Systems," Ph.D. Dissertation, Dept. of Aeronautics and Astronautics, Massachusetts Institute of Technology, Cambridge, MA, Feb. 1991.

[9] Johnson, W., "Self-Tuning Regulators for Multi-Cyclic Control of Helicopter Vibration," NASA TP 1996, March 1982.

[10] Patt, D., Liu, L., Chandrasekar, J., Bernstein, D. S., and Friedmann, P. P., "Higher-Harmonic-Control Algorithm for Helicopter Vibration Reduction Revisited," *Journal of Guidance, Control, and Dynamics*, Vol. 28, No. 5, Sept.–Oct. 2005, pp. 918–930. doi:10.2514/1.9345

[11] Friedmann, P. P., and Millott, T. A., "Vibration Reduction in Rotorcraft Using Active Control: A Comparison of Various Approaches," *Journal of Guidance, Control, and Dynamics*, Vol. 18, No. 4, July–Aug. 1995, pp. 664–673. doi:10.2514/3.21445

[12] Mannchen, T., and Well, K. H., "Helicopter Vibration Reduction and Damping Enhancement Using Individual Blade Control," *Journal of Guidance, Control, and Dynamics*, Vol. 27, No. 5, Sept.–Oct. 2004, pp. 760–766. doi:10.2514/1.12598

[13] Cribbs, R., and Friedmann, P. P., "Actuator Saturation and its Influence on Vibration Reduction by Actively Controlled Flaps," 42nd AIAA/ASME/ASCE/AHS/ASC Structures, Structural Dynamics, and Materials Conference and Exhibit, AIAA Paper 2001-1467, Seattle, WA, 16–19 April 2001.

[14] Liu, L., Friedmann, P. P., Kim, I., and Bernstein, D. S., "Simultaneous Vibration Reduction and Performance Enhancement in Rotorcraft Using Actively Controlled Flaps," 47th AIAA/ASME/ASCE/AHS/ASC Structures, Structural Dynamics, and Materials Conference, AIAA Paper 2006-1861, Newport, RI, 1–4 May 2006.

[15] Nixon, M. W., Kvaternik, R. G., and Settle, T. B., "Tiltrotor Vibration Reduction Through Higher Harmonic Control," NASA TM-112427, 1997.

[16] Knospe, C. R., Hope, R. W., Fedigan, S. J., and Williams, R. D., "Experiments in the Control of Unbalance Response Using Magnetic Bearings," *Mechatronics*, Vol. 5, No. 4, 1995, pp. 385–400. doi:10.1016/0957-4158(95)00015-W

[17] Mettin, R., and Kurz, T., "Optimized Periodic Control of Chaotic Systems," *Physics Letters A*, Vol. 206, No. 5–6, Oct. 1995, pp. 331–339. doi:10.1016/0375-9601(95)00644-I

[18] Anusonti-Inthra, P., Gandhi, F., and Miller, L., "Reduction of Helicopter Vibration Through Cyclic Control of Variable Orifice Dampers," *Aeronautical Journal*, Vol. 107, No. 1077, Nov. 2003, pp. 657–672.

[19] Kamath, G. M., Wereley, N. M., and Jolly, M. R., "Characterization of Magnetorheological Helicopter Lag Dampers," *Journal of the American Helicopter Society*, Vol. 44, No. 3, 1999, pp. 234–248. doi:10.4050/JAHS.44.234

[20] Zhao, Y., Choi, Y.-T., and Wereley, N. M., "Semi-Active Damping of Ground Resonance in Helicopters Using Magnetorheological Dampers," *Journal of the American Helicopter Society*, Vol. 49, No. 4, 2004, pp. 468–482.

[21] Eyres, R. D., "Vibration Reduction in Helicopters Using Lag Dampers," Ph.D. Dissertation, Department of Aerospace Engineering, Univ. of Bristol, Bristol, United Kingdom, Jan. 2005.

[22] Titurus, B., and Lieven, N. A. J., "Model Validation and Experimentally Driven Hydraulic Damper Model Refinement," *Proceedings of the International Conference on Noise and Vibration Engineering 2008*, Vols. 1–8, Katholieke Univ. Leuven, Leuven, Belgium, 2008, pp. 967–978.

[23] Hu, W., Wereley, N. M., Chemouni, L., and Chen, P. C., "Semi-Active Linear Stroke Magnetorheological Fluid-Elastic Helicopter Lag Damper," *Journal of Guidance, Control, and Dynamics*, Vol. 30, No. 2, 2007, pp. 565–575. doi:10.2514/1.24033

[24] Hu, W., and Wereley, N. M., "Rate-Dependent Elastoslide Model for Magnetorheological Damper," *Journal of Guidance, Control, and Dynamics*, Vol. 31, No. 3, 2008, pp. 479–489. doi:10.2514/1.32732

[25] Merritt, H. E., *Hydraulic Control Systems*, Wiley, New York, 1967, Chaps. 2, 3, 5.

[26] Mitchell, A. H., and Johnson, K. L., "Simulation of a Hydraulic Actuator," *IBM Journal of Research and Development*, Vol. 8, No. 3, July 1964, pp. 329–334.

[27] Yao, B., Bu, F., Reedy, J., and Chiu, G. T. C., "Adaptive Robust Motion Control of Single-Rod Hydraulic Actuators: Theory and Experiments," *IEEE/ASME Transactions on Mechatronics*, Vol. 5, No. 1, March 2000, pp. 79–91. doi:10.1109/3516.828592

[28] Audenino, A. L., and Belingardi, G., "Modelling the Dynamic Behaviour of a Motorcycle Damper," Proceedings of the Institution of Mechanical Engineers. *Proceedings of the Institution of Mechanical Engineers. Part D: Journal of Automobile Engineering*, Vol. 209, No. 4, 1995, pp. 249–262. doi:10.1243/PIME_PROC_1995_209_212_02

[29] Lee, C. T., and Moon, B. Y., "Simulation and Experimental Validation of Vehicle Dynamic Characteristics for Displacement-Sensitive Shock Absorber Using Fluid-Flow Modelling," *Mechanical Systems and Signal Processing*, Vol. 20, No. 2, Feb. 2006, pp. 373–388. doi:10.1016/j.ymssp.2004.09.006

[30] Hong, S.-R., Wang, G., Hu, W., and Wereley, N. M., "Liquid Spring Shock Absorber with Controllable Magnetorheological Damping," *Proceedings of the Institution of Mechanical Engineers. Part D: Journal of Automobile Engineering*, Vol. 220, No. 8, 2006, pp. 1019–1029. doi:10.1243/09544070JAUTO74

[31] Duym, S. W. R., "Simulation Tools, Modelling, and Identification for an Automotive Shock Absorber in the Context of Vehicle Dynamics," *Vehicle System Dynamics*, Vol. 33, No. 4, April 2000, pp. 261–285. doi:10.1076/0042-3114(200004)33:4;1-U;FT261

[32] Surace, C., Worden, K., and Tomlinson, G. R., "On the Non-Linear Characteristics of Automotive Shock Absorbers," *Proceedings of the Institution of Mechanical Engineers. Part D: Journal of Automobile Engineering*, Vol. 206, No. 1, 1992, pp. 3–16. doi:10.1243/PIME_PROC_1992_206_156_02

[33] Ferreira, J. A., Gomes de Almeida, F., and Quintas, M. R., "Semi-Empirical Model for a Hydraulic Servo-Solenoid Valve," *Proceedings of the Institution of Mechanical Engineers. Part I: Journal of Systems and Control Engineering*, Vol. 216, No. 3, 2002, pp. 237–248. doi:10.1243/095965102320005409

[34] MATLAB, Software Package, Ver. 7.4, MathWorks, Natick, MA, 2007.

R. Kapania
Associate Editor